Volcanic evolution of an ultraslow-spreading ridge

H. H. Stubseid*, A. Bjerga, H. Haflidason and R. B. Pedersen

Center for Deep Sea Research and Department of Earth Science, University of Bergen, Allégaten 41, N-5007 Bergen, Norway

Corresponding author. E-mail:* havard.stubseid@uib.no

Supplementary Information

High-resolution bathymetry and sub-bottom profiler

High-resolution bathymetry was collected using AUV mounted Kongsberg EM 2040 multibeam echosounder at 200 kHz with a ping rate of 10 Hz. Beam angle was set to 45/45 giving coverage of 150/150 m. The backscatter db signal was acquired simultaneously as the bathymetry parameter. The AUV had a flight height of ~50-80 meters and a speed of approximately 3.5-4 knots. Onboard data processing was done by Ocean Infinity. All the maps were gridded and visualized with a resolution of 1 m using the Fledermaus software.

Sub-bottom profiler data were acquired using an EdgeTech Commander version 8.7.3. Penetration of sub-bottom profiler data is limited to ~100 m depth into the sediments and the vertical resolution of the recorded data is determined by the bandwidth of the echo-sounder system and the secondary frequency of parametric systems estimated to be between 30 and 50 cm. During data collection, 100-180 m of vertical data were logged, limiting the resolution of the upper meters of sediment cover. Processing of raw data was done using the Chesapeake Technology software SonarWiz 7. All data were corrected for navigation using updated navigation files extracted from Eiva navigation software. Further, post-processing was done in SonarWiz such as aggregation of files, bottom-tracking, blanking of water-column, and applying of gain. Top basalt reflectors were manually drawn on each line representing the base of the sediment cover. Only areas with visible sediments were interpreted. Areas with no sediments (or too little to be seen in the data) represent approximately 10% of the data set.

Data analysis and areal calculations

All interpretations of backscatter and sub-bottom data were done on top of high-resolution bathymetry for better control of the terrain and locations. Sediment thicknesses was calculated using the "compute thickness" function in SonarWiz, between the manually interpreted top-basalt reflector and the digitized corrected bottom-track, with a down-sampling interval of 5 on each reflector. Based on the manual interpretation and the resolution of the collected data, we estimate an uncertainty of +/- 0.5 m in the sediment thickness. The calculated sediment thicknesses were exported as XYZ (latitude, longitude, and sediment thickness) text files and gridded to a isopach map in the Fledermaus software with a cell size of 175 m, giving the average sediment thickness for an area of 0.03 km^2. The cell size was primarily based on the spacing between the lines that were up to 800 m. A final gridded surface was draped onto the underlying bathymetry for visualization of the sediment distribution (Fig. S1). The accuracy of the gridding was assessed by acquiring direct measurements of sediment thicknesses from SBP data, correlated with the length of actual cores, and compared with backscatter and bathymetric maps using the 3D function of Fledermaus (Fig. S2, S3 & S4). We find a near-perfect match between the backscatter maps and the isopach map generated from the interpretation of sub-bottom profiles strengthening the method.

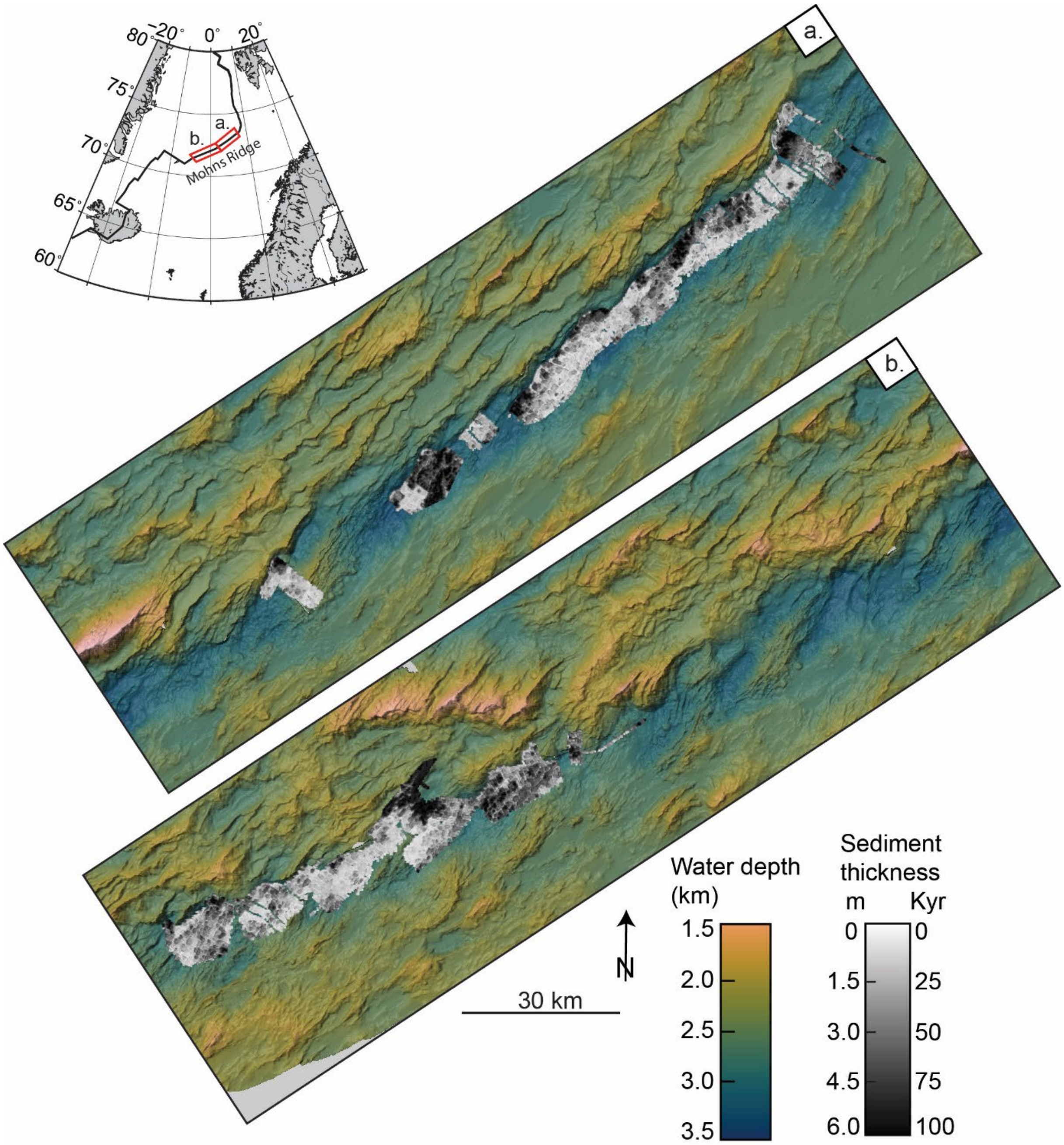

Supplementary Figure S1: Overview of the main part of the Mohns Ridge showing the entire isopach map. **a.** The northern part of the isopach map, with sediment the thickness draped onto 70 m resolution bathymetry. Note that the three southernmost surveyed areas within this figure is missing from Fig. 1 in the main text. Therefore, all data is included here. **b.** shows the southernmost part of the isopach map. All collected high-resolution bathymetry and back-scatter data cover the same area as for the sediment thicknesses.

Area calculations from the isopach map were performed using thresholding of a global grayscale image in ImageJ. A five-scale image of the sediment thicknesses was created in Fledermaus software representing every 1.5 m of sediments before the total area of each class was measured. Thresholding of each class was completed prior to all calculations giving a range for each shade of gray as follows: 0-1.5 m = RGB 235-255, 1.5-3 m = RGB 195-235, 3-4.5 m = RGB 160-195, 4.5-6 m = RGB 60-160, >6 m = RGB 10-60. Uncertainty related to setting a global scale was calculated to 1%. Areas representing only one pixel were excluded from the calculations. A deviation of 0.01% on the total area is present before and after thresholding. The same procedure was applied to calculate the sediment distribution of three different sub areas: AVRs (defined as bathymetric highs), AVR-flanks (from the bathymetric high to the rift bounding fault) and non-transform offsets (areas in between orthogonal spreading cells). All calculations of the sediment thickness and the age of underlaying lava (each 1.5 m are equal to 25 Kyr) are presented in Fig. 3 in the main text.

Sediment cores and radiocarbon dating

A comprehensive coring campaign was conducted to establish and evaluate the sedimentation rates for the entire Mohns Ridge. A total of 21 gravity cores were collected during cruises with RV G.O Sars in 2020 and 2021 (Fig. 2 in main text and Supplementary Table S1). Only one core, GS20-230-19GC, retrieved no sediments. Gravity cores were collected using a 5 m steel tube hitting the seafloor with a speed of approximately 1 m per second. Cores were cut into sections, labeled, and placed in cold storage. Further processing was conducted at the EarthLab, Department of Earth Science at the University of Bergen. Every core section was split into two halves and scanned on the ITRAX XRF core scanner combining X-ray reflectance (XRF), radiographic X-ray imaging, and optical imaging (RGB, 3x3000 pictures). The element composition was measured every 2nd mm.

Supplementary Table S1: Overview of sediment cores. The table includes map ID, core ID, latitude, longitude, core length and water depth for all the collected sediment cores.

Map ID	Core ID	Latitude	Longitude	Core Length (cm)	Water depth (m)
1	GS20-230-03GC	72° 17.6913' N	01° 40.8273' E	308	2650
2	GS20-230-06GC	72° 29.6665' N	02° 30.4937' E	197	3000
3	GS20-230-07GC	72° 44.9100' N	03° 56.5621' E	80	2500
4	GS20-230-09GC	72° 45.2560' N	03°49.8750' E	62	3050
5	GS20-230-10GC	72° 45.3210' N	03°49.9760' E	129	3026
6	GS20-230-11GC	72° 47.4420' N	03°56.6080' E	313	2490
7	GS20-230-12GC	72° 44.6755' N	04° 18.1880' E	135	2676
8	GS20-230-13GC	72° 55.2010' N	04° 58.8690' E	345	3000
9	GS20-230-14GC	73° 01.2580' N	05° 29.5430' E	272	3000
10	GS20-230-15GC	73° 10.3810' N	06° 12.5630' E	275	3360
11	GS20-230-16GC	73° 13.3730' N	06°32.7790' E	323	3360
12	GS20-230-17GC	73° 16.0380' N	06° 46.9960' E	134	3010
13	GS20-230-18GC	73° 18.7400' N	06° 49.9290' E	385.5	3137
14	GS20-230-19GC	73° 27.2990' N	07° 12.5550' E	0	2764
15	GS20-230-20GC	73° 23.1130' N	07° 19.0510' E	294	2560
16	GS20-230-21GC	73° 20.2150'N	07° 24.9140' E	286	3000
17	GS21-235-GC04	71° 54.7540' N	01° 18.7970' W	349	2770
18	GS21-235-GC05	72° 05.3620' N	00° 07.8560' W	440	3122
19	GS21-235-GC06	72° 44.9210' N	03° 49.5950' E	150	3085
20	GS21-235-GC07	72° 45.3630' N	03° 49.6340' E	70	3010
21	GS21-235-GC08	72° 45.3240' N	03° 49.9790' E	120	3010

Five selected cores were sub-sampled, sieved, and cleaned before specimens of the planktonic foraminifera species N. pachyderma (sin) were handpicked for radiocarbon dating (Fig. S4 and S5). Radiocarbon dating analyzes were performed at the Radiocarbon Dating Laboratory, Department of Geology, Lund University, Sweden. Ages were corrected for total isotopic fractionation and converted to calendar years using the Marine20 calibration curve[1]. The age results were correlated and compared with the elemental record from the remaining 15 cores, providing a robust framework for the age model (Fig. S7). Our results reveal a sedimentation rate of on average 6 cm/Ka for the rift valley floor of the Mohns Ridge. This is significantly higher than in the open ocean of the Norwegian-Greenland Sea with a sedimentation rate in the order of 2-4 cm/Ka [2-4].

Several studies have suggested that age-to-depth ratios in sediment cores might not be accurate due to potential disturbance from re-sedimentation and bioturbation [5-7] . In high-latitude deep sea areas the disturbance from bioturbation can be high owing to generally low sedimentation rates. To evaluate the extent and magnitude of vertical mixing in these areas tephra particles have been applied as a tracer to document the rate and quantity of bioturbation. The vertical distribution of the volcanic glass particles in the studied cores shows that effective mixing of the sediments does not exceed 2–3 cm and the original layer is not markedly displaced. The amplitude of the original signal is therefore only slightly smoothed [8,9].

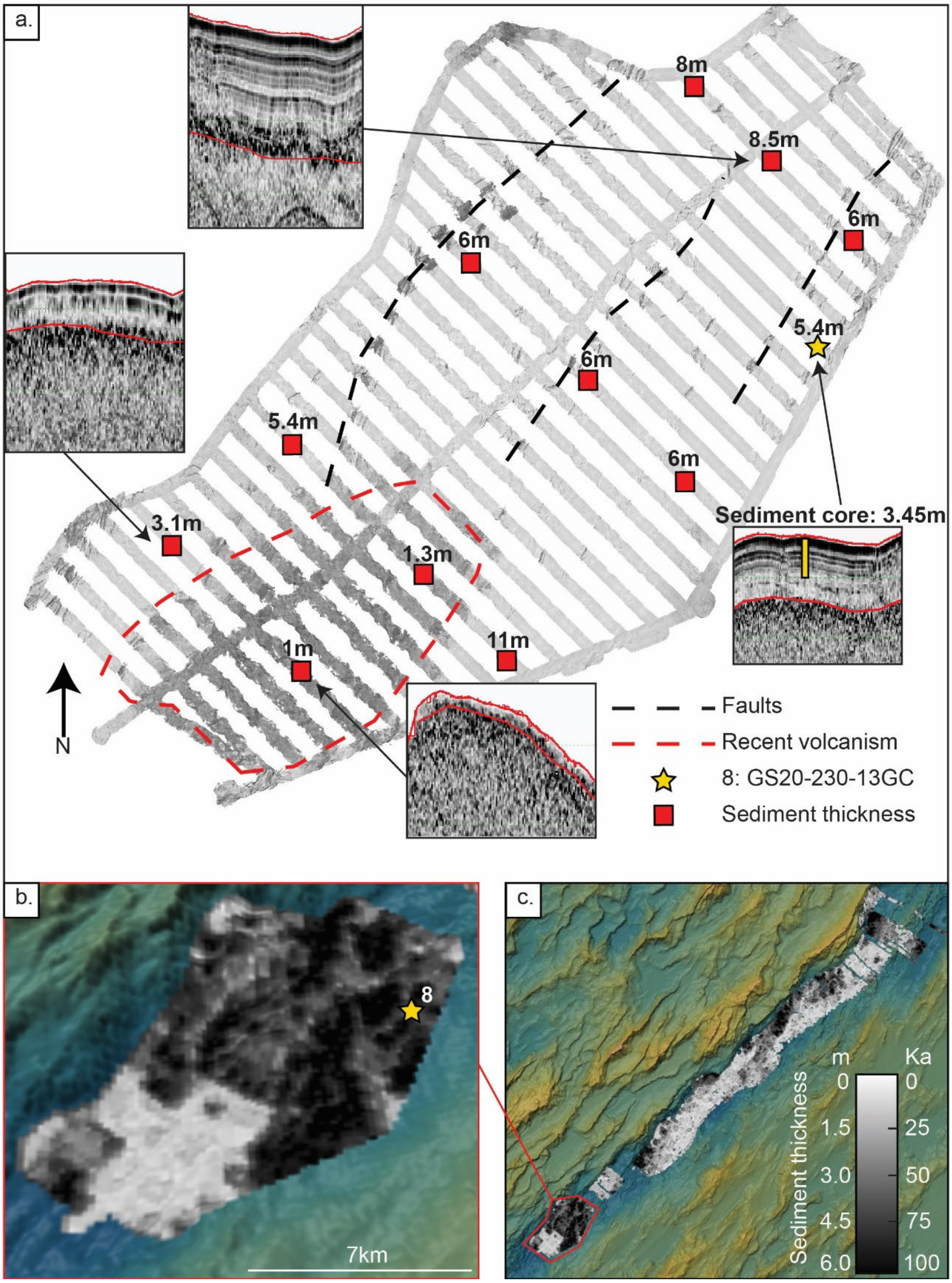

Supplementary Figure S2: Sediment thicknesses and backscatter map for the area of core 8. a. Backscatter map (AUV data) of 1m resolution is shown to further confirm the degree of sedimentation. Accurate measurements of the sediment thicknesses, acquired from the sub-bottom profiles, are shown as red squares in various locations. Insets of the seismic lines are used to visualize the sedimentary deposits. GS20-230-13GC is marked as a yellow star with its exact length presented within the seismic profile for the sampled area. **b.** The figure shows the sediment distribution and age of the volcanic crust for a sub-area of the northern zone. **c.** Overview of the northern part of the isopach map. The detailed sub area is marked with red lines.

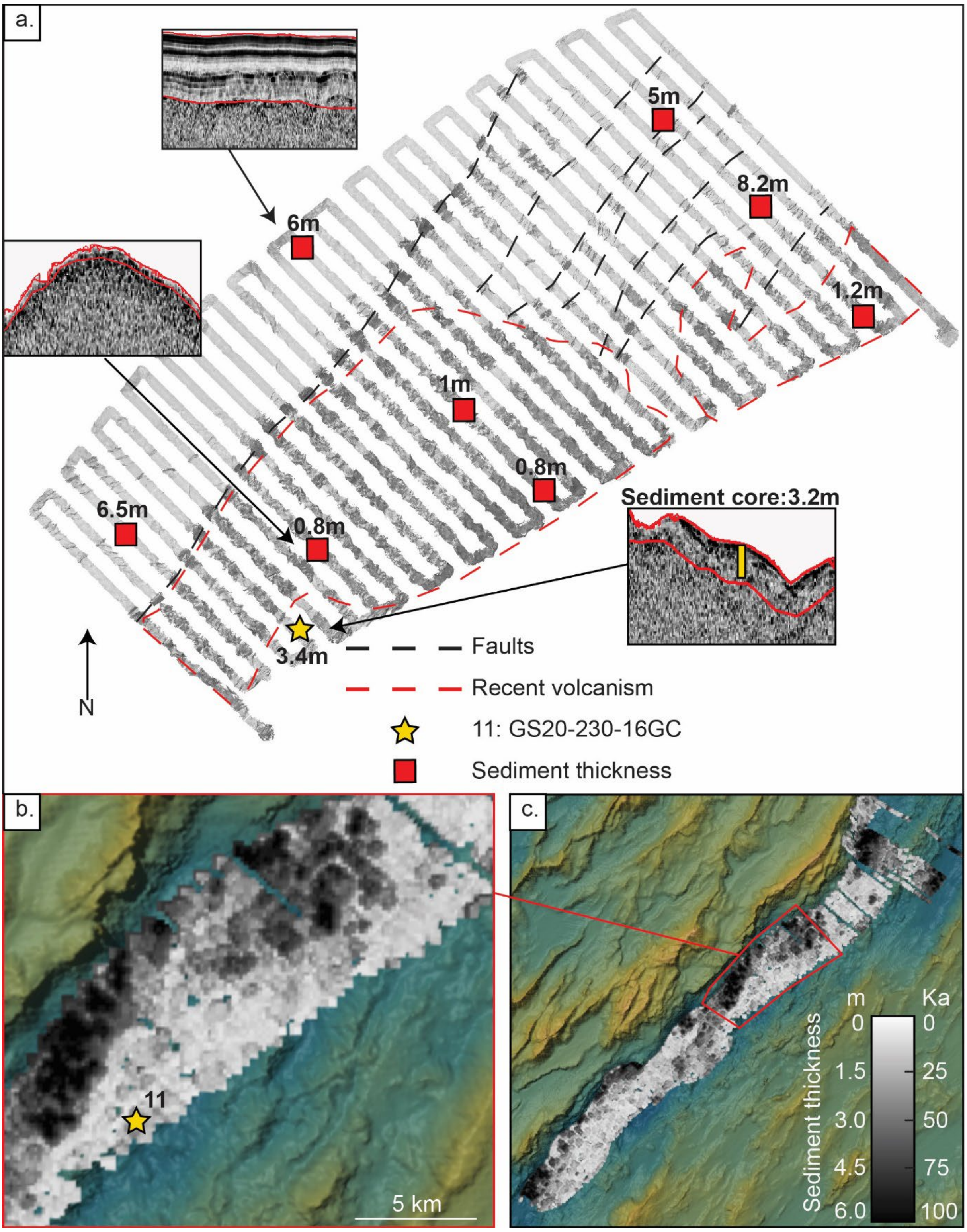

Supplementary Figure S3: Sediment thicknesses and backscatter map for the area of core 11. a. Backscatter map (AUV data) of 1m resolution is shown to further confirm the degree of sedimentation. Accurate measurements of the sediment thicknesses, acquired from the sub-bottom profiles, are shown as red squares in various locations. Insets of the seismic lines are used to visualize the sedimentary deposits. GS20-230-16GC is marked as a yellow star with its exact length presented within the seismic profile for the sampled area. **b.** The figure shows the sediment distribution and age of the volcanic crust for a sub-area of the northern zone. **c.** Overview of the northern part of the isopach map. The detailed sub area is marked with red lines.

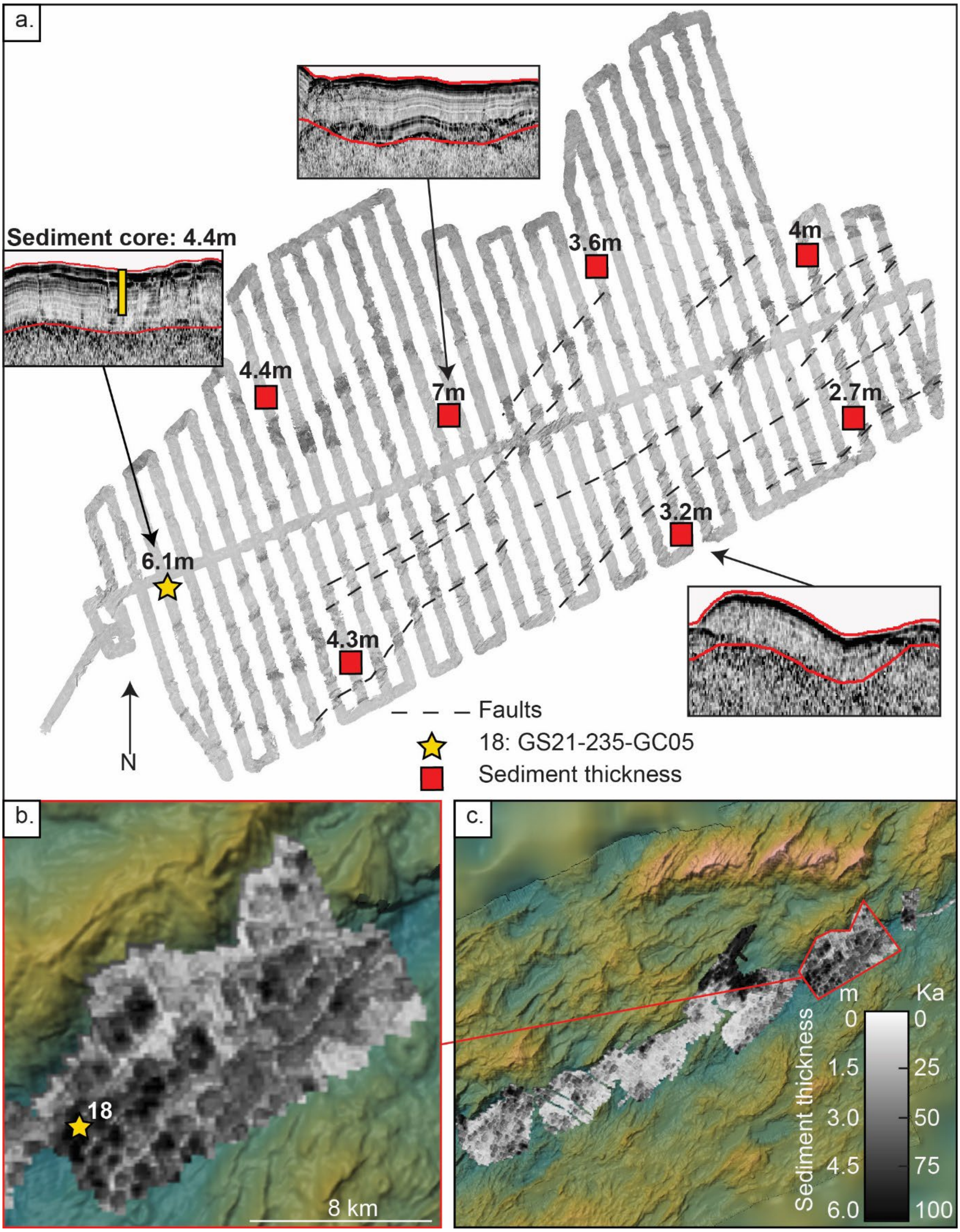

Supplementary Figure S4: Sediment thicknesses and backscatter map for the area of core 18. a. Backscatter map (AUV data) of 1m resolution is shown to further confirm the degree of sedimentation. Accurate measurements of the sediment thicknesses, acquired from the sub-bottom profiles, are shown as red squares in various locations. Insets of the seismic lines are used to visualize the sedimentary deposits. GS21-235-GC05 is marked as a yellow star with its exact length presented within the seismic profile for the sampled area. **b.** The figure shows the sediment distribution and age of the volcanic crust for a sub-area of the northern zone. **c.** Overview of the northern part of the isopach map. The detailed sub area is marked with red lines.

Supplementary Table 2: Overview of marine AMS ^{14}C-dates of the 5 dated cores. The ^{14}C dates are calibrated using the Marine20 calibration model (Heaton et al., 2020).

Map ID.	Core No.	Lab. ID	Depth in core (cm)	Material	^{14}C (BP)	$^{14}C \pm 1\delta$	Cal. BP (1δ) Median	Median (interval)
1	GS20-230-03GC	LuS 17211	11.0 - 12.0	*N. pach* (sin)	9 350	50	**10 000**	(9898 -10116)
		LuS 17212	31.0 - 32.0	*N. pach* (sin)	14 380	100	**16 580**	(16398-16751)
		LuS 17213	51.0 - 52.0	*N. pach* (sin)	18 990	120	**22 070**	(21920-22240)
		LuS 17214	71.0 - 72.0	*N. pach* (sin)	25 290	210	**28 655**	(28425-28915)
		LuS 17426	110.5 - 111.5	*N. pach* (sin)	44 600	+1200/-1000	**46 485**	(45109-47560)
		LuS 17427	165.0 - 166.0	*N. pach* (sin)	36 500	400	**40 535**	(40195-40906)
		LuS 17428	209.0 - 210.0	*N. pach* (sin)	44 700	+1200/-1000	**46 465**	(45365-47395)
8	GS20-230-13GC	LuS 17215	55.0 - 56.0	*N. pach* (sin)	9 035	50	**9 550**	(9462-9633)
		LuS 17216	100.0 - 101.0	*N. pach* (sin)	17 350	120	**20 055**	(19872-20241)
		LuS 17477	155.5 - 156.5	*N. pach* (sin)	29 700	200	**33 375**	(33116-33640)
		LuS 17478	235.0 - 236.0	*N. pach* (sin)	40 700	+1000/-900	**43 255**	(42475-43878)
11	GS20-230-16GC	LuS 17205	15.0 - 16.0	*N. pach* (sin)	3 390	35	**3 075**	(2985-3164)
		LuS 17206	30.0 - 31.0	*N. pach* (sin)	6 500	40	**6 770**	(6677-6857)
		LuS 17207	46.0 - 47.0	*N. pach* (sin)	8 615	55	**9 075**	(8979-9183)
		LuS 17208	55.0 - 56.0	*N. pach* (sin)	9 120	45	**9 650**	(9538-9731)
		LuS 17209	106.0 - 107.0	*N. pach* (sin)	16 430	100	**18 940**	(18790-19079)
		LuS 17210	157.0 - 158.0	*N. pach* (sin)	24 440	190	**27 745**	(27514-27951)
		LuS 17479	225.0 - 225.5	*N. pach* (sin)	30 200	300	**33 885**	(33601-34216)
		LuS 17480	272.0 - 273.0	*N. pach* (sin)	40 700	+1000/-900	**43 255**	(42475-43876)
16	GS20-230-21GC	Beta-647321	140.5 - 141.5	*N. pach* (sin)	15 570	50	**17 990**	(17828-18153)
		Beta-647322	209.5 - 210.5	*N. pach* (sin)	25 370	100	**28 745**	(28606-28886)
18	GS21-235-GC05	LuS 17483	168.0 - 169.0	*N. pach* (sin)	15 920	70	**18 410**	(18272-18544)
		LuS 17484	286.0 - 287.0	*N. pach* (sin)	35 600	500	**39 790**	(39325-40232)

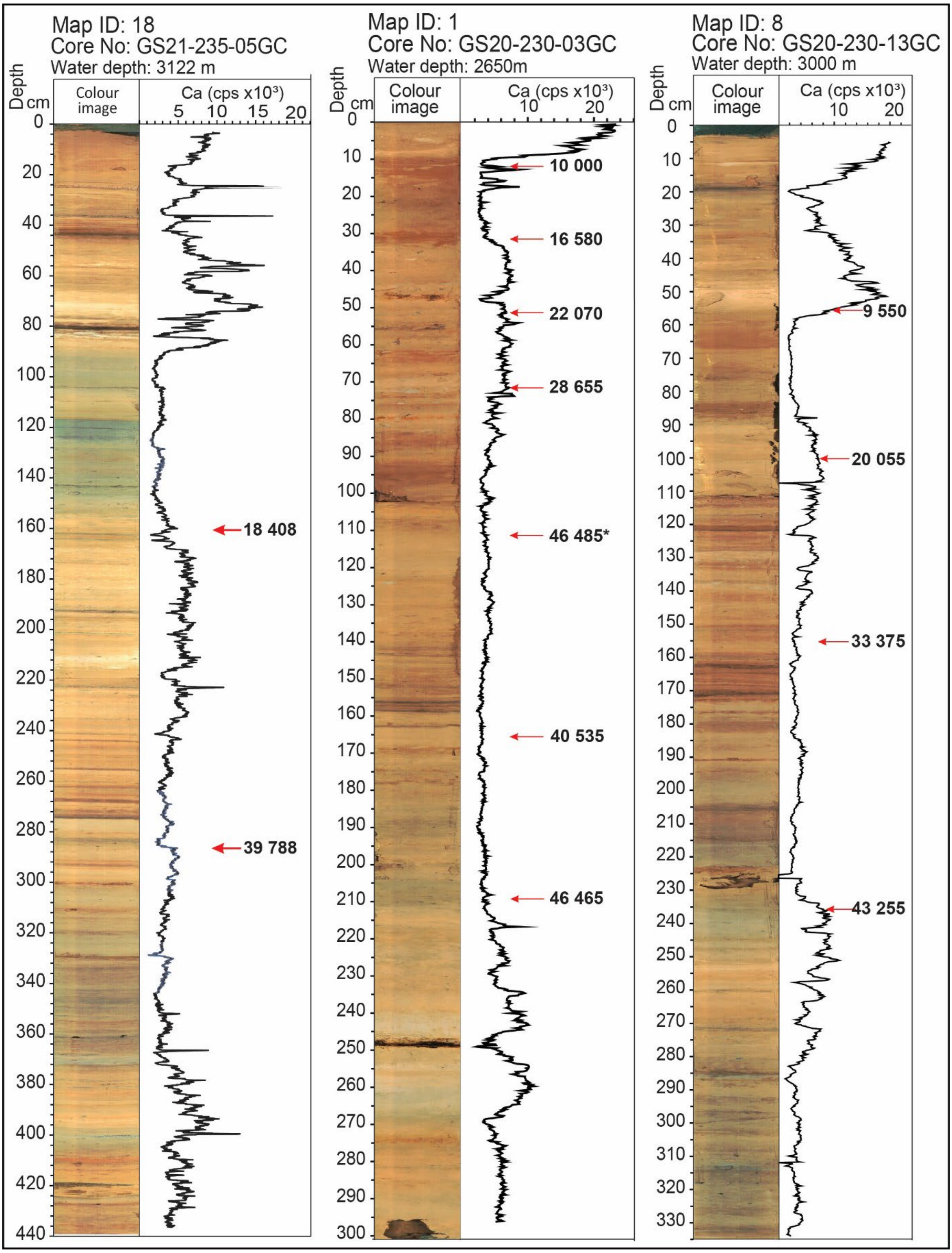

Supplementary Figure S5: Overview of 3 dated cores. The figure shows the colour image of three of the dated cores, from south to north: nr. 18 (GS21-235-05GC), nr. 1 (GS20-230-13GC) and nr. 8 (GS20-230-13GC). Note that core nr. 1 was over penetrated and the top part of the core is missing. The Ca curve, measured every 2nd mm using XRF element scanner, is presented together with the acquired ^{14}C dates for each core (details in Table S2). Note that core nr 1 exhibit one old-over-younger age (46 485*). This is outside the age trend for the rest of the core, and an isolated data point at this age is not reliable as it is on the limit of the method.

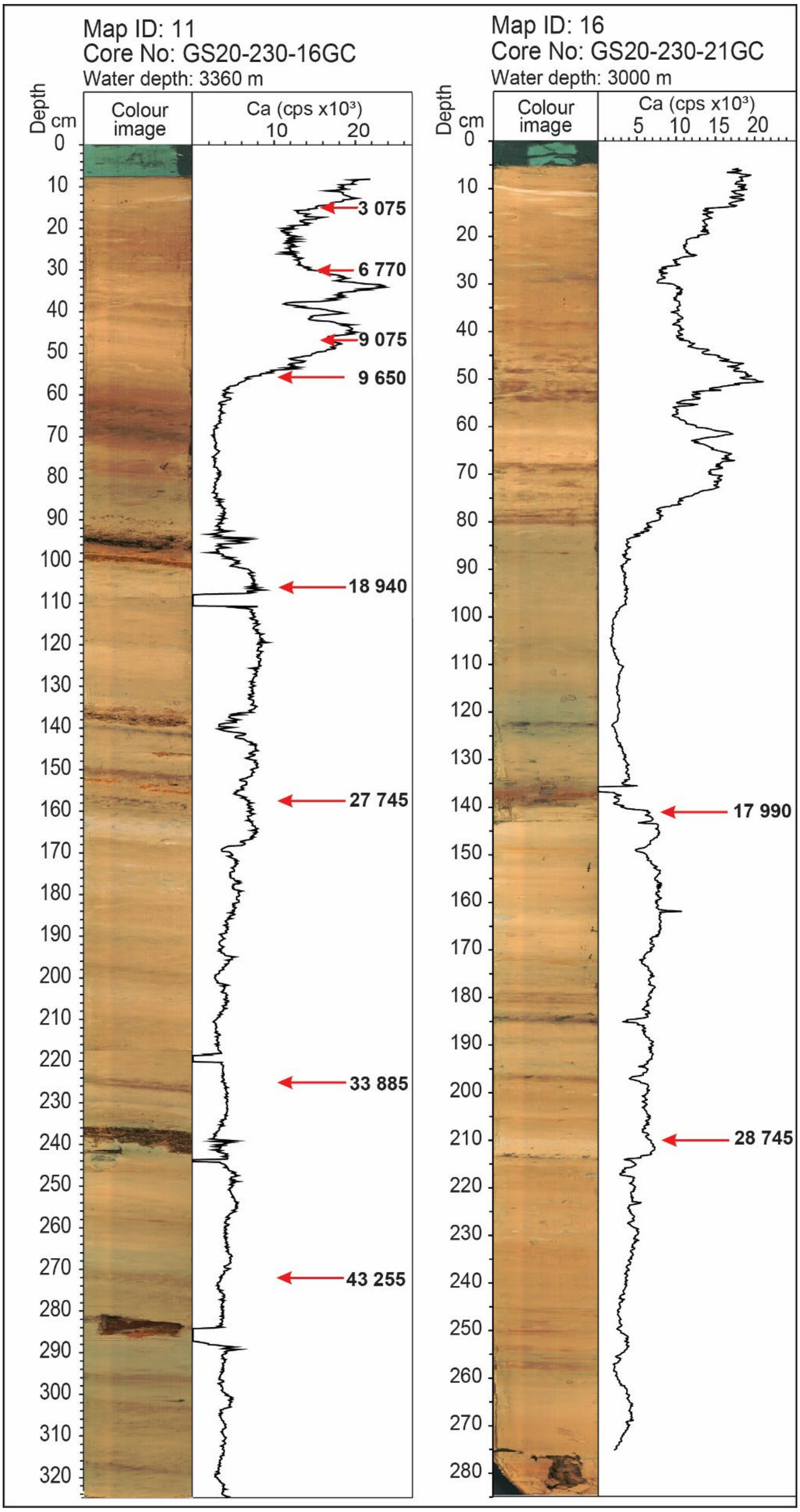

Supplementary Figure S6: Overview of 2 northernmost dated cores. The figure shows the colour image of the two northernmost dated cores: nr. 11 (GS20-230-16GC) and nr. 16 (GS20-230-21GC). The Ca curve, measured every 2nd mm using XRF element scanner, is presented together with the acquired ^{14}C dates for each core (details in Table S2).

The Ca geochemical composition (semi-quantitative) was determined by the ITRAX XRF core scanning system at a spatial resolution of 2 mm, using a molybdenum X-ray tube at the EarthLab core scanning facility, the University of Bergen. The Ca-counts represents the concentration of carbon preserved in the marine core stratigraphy where the variability reflects the productivity in the surface open ocean from calcareous planktons like planktonic forams and coccoliths and the variability of the regional paleo oceanographic conditions [10-12]. Therefore, the Ca curve is used for correlation between the different cores (Fig. S7) and to establish the sedimentation rate by comparing the chemo stratigraphy and using C^{14} ages from core nr. 1, 8, 11, 16 and 18.

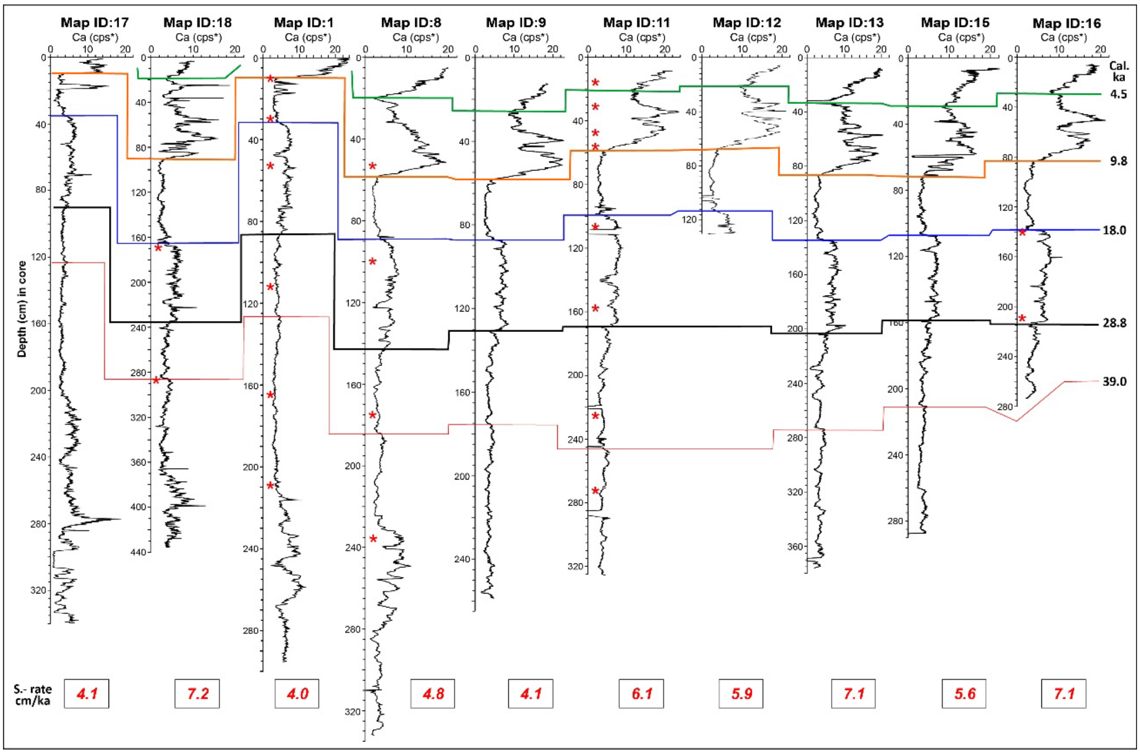

Supplementary Figure S7: Compilation of Ca-curve for 10 of the studied cores. The figure shows the XRF element scanning of Ca for 10 of the studied cores. The cores are sorted geographically from south to north along the ridge and the average sedimentation rate is reported as red numbers for each core. Here, anomalies in the Ca curve that are present inn all the cores are used to correlate their stratigraphy. ^{14}C ages, presented in Fig. S5, Fig S6 and Table S2, from the five dated cores (nr. 1, 8, 11, 16 and 18) are used to date the different anomalies and to establish the sedimentation rates for the cores. Red stars mark the location of all dated samples. This further strengthens our age model and verifies an average sedimentation rate of 6cm/Ka for the entire rift valley. Note that the top part of core 17 and 1 is lost due to over penetration.

References

1 Heaton, T. J. *et al.* Marine20—the marine radiocarbon age calibration curve (0–55,000 cal BP). *Radiocarbon* **62**, 779-820 (2020).

2 Fronval, T. & Jansen, E. Eemian and early Weichselian (140–60 ka) paleoceanography and paleoclimate in the Nordic seas with comparisons to Holocene conditions. *Paleoceanography* **12**, 443-462 (1997).

3 Fronval, T., Jansen, E., Haflidason, H. & Sejrup, H. P. Variability in surface and deep water conditions in the Nordic seas during the last interglacial period. *Quaternary Science Reviews* **17**, 963-985 (1998).

4 Koç, N. & Jansen, E. Response of the high-latitude Northern Hemisphere to orbital climate forcing: Evidence from the Nordic Seas. *Geology* **22**, 523-526 (1994).

5 Clague, D. A. *et al.* Geologic history of the summit of Axial Seamount, Juan de Fuca Ridge. *Geochemistry, Geophysics, Geosystems* **14**, 4403-4443 (2013).

6 Portner, R. A., Clague, D. A., Helo, C., Dreyer, B. M. & Paduan, J. B. Contrasting styles of deep-marine pyroclastic eruptions revealed from Axial Seamount push core records. *Earth and Planetary Science Letters* **423**, 219-231 (2015).

7 Zuhr, A. M. *et al.* Age-Heterogeneity in Marine Sediments Revealed by Three-Dimensional High-Resolution Radiocarbon Measurements. *Frontiers in Earth Science* **10** (2022).

8 Haflidason, H., Eiriksson, J. & Kreveld, S. V. The tephrochronology of Iceland and the North Atlantic region during the Middle and Late Quaternary: a review. *Journal of Quaternary Science: Published for the Quaternary Research Association* **15**, 3-22 (2000).

9 Sjøholm, J., Sejrup, H. P. & Furnes, H. Quaternary volcanic ash zones on the Iceland Plateau, southern Norwegian Sea. *Journal of Quaternary Science* **6**, 159-173 (1991).

10 Brendryen, J., Haflidason, H. & Sejrup, H. P. Norwegian Sea tephrostratigraphy of marine isotope stages 4 and 5: prospects and problems for tephrochronology in the North Atlantic region. *Quaternary Science Reviews* **29**, 847-864 (2010).

11 Helmke, J. P., Bauch, H. A., Röhl, U. & Mazaud, A. Changes in sedimentation patterns of the Nordic seas region across the mid-Pleistocene. *Marine Geology* **215**, 107-122 (2005).

12 Rothwell, R. G. in *Micro-XRF studies of sediment cores* 25-102 (Springer, 2015).